

Artículo de investigación

## Hydrodechloration of diclofenac using nanoparticles of zerovalent iron and nZVI supported

### hidrocloración de diclofenaco usando nanoparticulas de hierro zerovalente ( nZVI) y nZVI soportado

Luna López <sup>1</sup>, Paula Ramírez <sup>2</sup> & Maria H. Brijaldo <sup>3</sup> ✉

<sup>1</sup>Facultad de Ciencias Químicas, División de Estudios de Posgrado, Universidad Autónoma de Nuevo León, Av. Universidad, San Nicolás de los Garza, N.L. C.P. 66455, México

<sup>2</sup>Maestría en Química, Facultad de Ciencias, Universidad Pedagógica y Tecnológica de Colombia UPTC, Avenida Central del Norte, vía Paipa, Tunja, Boyacá, 150003, Colombia.

<sup>3</sup>Escuela de Ciencias Administrativas y Económicas, Facultad de Estudios a Distancia, Universidad Pedagógica y Tecnológica de Colombia, Av. Central Norte 39-115 Tunja, 150003, Colombia.

Recepción: 10-oct-2024      Aceptado: 8-nov-2024

#### Abstract

Diclofenac (DFC) is well known as a non-steroidal anti-inflammatory drug and its high production and consumption make it an emerging pollutant. DFC tends to accumulate in aquatic systems inducing toxicity along food chains. Developing alternatives for the elimination of emerging pollutants must be one of the challenges of environmental chemistry, so this research focused on the catalytic hydrodechlorination (HDC) of diclofenac (DCF) using zero-valent iron nanoparticles (nZVI) supported on alumina ( $Al_2O_3$ ) and activated carbon (AC). The catalysts were obtained from  $Fe(NO_3)_3 \cdot 9H_2O$  by two reduction methods: extract of pine of the Cypress variety (*Cupressus sempervirens*) and the second using  $NaBH_4$ . The catalysts were characterized by studying the physicochemical and morphological properties characterized by the techniques of X-ray diffraction (XRD), X-ray photoelectron spectroscopy (XPS), Transmission Electron Microscopy (TEM) and Raman spectroscopy. Catalytic activity tests were performed by using of DCF hydrodechlorination reactions with each catalyst, with constant monitoring with the high-performance liquid chromatography (HPLC) technique. The nZVI-P/CA and nZVI-P/ $Al_2O_3$  catalysts presented good dispersion and activity, with conversions close to 100%. The nZVI-P/CA showed greater selectivity towards the desired products, while the nZVI-P/ $Al_2O_3$  was more stable over time. This research addresses the environmental risk of bioaccumulation of this type of organochlorine compounds and proposes a promising solution for their treatment.

**Keywords:** Diclofenac; 2-Anilinophenylacetate; Hydrodechlorination; Zerovalent iron; Nanoparticles.

#### Resumen

El diclofenaco (DFC) es bien conocido como un medicamento antiinflamatorio no esteroideo y su alta producción y consumo lo convierten en un contaminante emergente. El DFC tiende a acumularse en sistemas acuáticos induciendo la toxicidad a lo largo de la cadena alimenticia. Desarrollando alternativas para la eliminación de contaminantes emergentes es uno de los desafíos más grandes de la química ambiental, de esta manera esta investigación esta enfocada en la hidrodecloración (HDC) de diclofenaco (DCF) usando nanoparticulas de hierro zerovalente (nZVI) soportadas en alumina ( $Al_2O_3$ ) y carbon activado (AC). Los catalizadores se obtuvieron a partir de  $Fe(NO_3)_3 \cdot 9H_2O$  mediante dos métodos de reducción: extracto de pino variedad Ciprés (*Cupressus sempervirens*) y la segunda usando  $NaBH_4$ . Los catalizadores se caracterizaron mediante el estudio de las propiedades fisicoquímicas y morfológicas caracterizadas por las técnicas de difracción de rayos X (XRD), espectroscopia fotoelectrónica de rayos X (XPS), microscopía electrónica de transmisión (TEM) y espectroscopia Raman. Las pruebas de actividad catalítica se realizaron mediante reacciones DCF HDC con cada catalizador, monitoreando constantemente con la técnica de cromatografía líquida de alta resolución (HPLC). Los catalizadores nZVI-P/CA y nZVI-P/ $Al_2O_3$  presentaron buena dispersión y actividad, con conversiones cercanas al 100%. El nZVI-P/CA mostró mayor selectividad hacia los productos deseados, mientras que el nZVI-P/ $Al_2O_3$  fue más estable en el tiempo. Esta investigación aborda el riesgo ambiental de la bioacumulación de este tipo de compuestos organoclorados y propone una solución prometedora para su tratamiento.

**Palabras Clave:** Diclofenaco, 2-anilínfenilacetato, hidrodecloración, hierro zerovalente, nanoparticulas.

## 1 Introduction

Since the ratification of the Stockholm and Rotterdam Conventions, the limited use of organochlorine compounds (COCs) has been promoted [1]. Since 2008, Colombia has been part of the group of countries that have adopted this initiative; however, it has been shown that COCs continue to be used nationally in agricultural activity and the production of plastics and electronic products [2]. The World Health Organization (WHO) has stated that COCs, such as vinyl chloride (PVC) and dioxin, insecticides (dichlorophenoxyethane (DDT)) and nonsteroidal anti-inflammatory drugs (NSAIDs), can be harmful to human health and the environment due to their bioaccumulation in aquatic ecosystems [3]. Thus, the WHO, together with the Ministry of Health and Social Protection of Colombia, have promoted the development of safe alternatives in the remediation processes of these compounds to reduce the risks caused by their exposure [4].

One of the most representative COCs is DCF used as NSAIDs and frequently detected in bodies of water along with other pharmacologically active compounds (CFAs). It is considered an emerging pollutant due to physicochemical properties such as solubility, bioaccumulation, persistence, biotransformation and toxicity, it is considered an emerging contaminant [5]. Diclofenac is a drug that can have harmful effects on aquatic organisms; according to an OpenMind article, it can poison trout in rivers and vultures that feed on the carcasses of cattle treated with the drug. Likewise, it can bioaccumulate, inducing toxicity throughout food chains [6]. Following this problem that DCF represents, different biological, thermal, photocatalytic, and oxidative degradation processes have been developed in the liquid phase. However, these procedures have proven to be quite expensive because they are inefficient and, therefore, require the implementation of catalysts based on noble metals.

According to Wildeman et al. [7], the microbiological degradation of DCF is quite difficult and therefore, new approaches have been sought to optimize this process. For this reason, Quan et al. [8] evaluated the catalytic capacity of Pd-based anaerobic granular sludges (Pd-GAL) during DCF degradation. Although these materials exhibit excellent catalytic behavior during degradation, they are quite expensive due to the use of palladium as a precursor. On the other hand, in the photocatalytic degradation of DCF, new catalysts based on graphitic carbon nitride ( $gC_3N_4$ ) doped with organometallic complexes (COMs) have been investigated, such as the photocatalysts prepared by Muelas-Ramos et al. [9] who used a COM containing Ti ( $NH_2$ -MIL-125) or Al-Ga- $\times$ Ag type coupled compounds, which were obtained and evaluated by Casillas et al., [10]. These modifications that have been made at the structural level of each photocatalyst have made it possible to avoid the rapid recombination of electron-hole pairs ( $e^- - h^+$ ) and, therefore, optimal results have been achieved during the degradation of DCF. However, some of these procedures are still quite expensive, and therefore, the development of more economical and efficient processes has been suggested.

From this perspective, catalytic hydrodechlorination (HDC) has been seen as a promising technology for the removal of CFAs. This process is based on the treatment of the pollutant

under an  $H_2$  atmosphere to generate the corresponding dechlorinated products and hydrochloric acid (Figure 1). Therefore, this process, significantly reduces the ecotoxicity of the effluent and avoid the formation of more harmful intermediates under ambient conditions [11]. Despite the great potential of HDC, there is little research during the last years and therefore, it is necessary to investigate this process in depth.

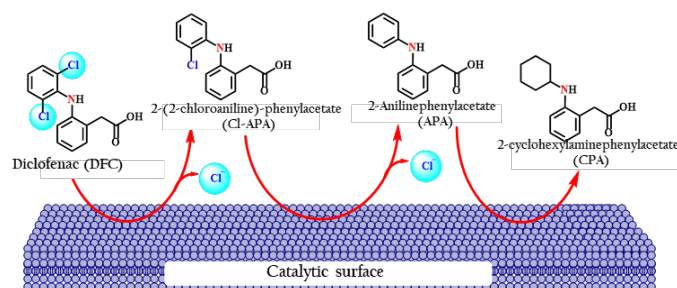


Figure 1: Proposed reaction pathway for the HDC of DCF. Adapted from Nieto-Sandoval et al. , [12]

Among the most representative investigations that have been addressed concerning the HDC of DCF, through heterogeneous catalytic processes, the study carried out by Lokteva et al. [13], in which monometallic Pd and bimetallic Pd-Fe catalysts (1% w/w Pd, 10% w/w Fe) were prepared by sequential impregnation (“-s”) and co-impregnation (“-c”) of  $Al_2O_3$  and  $SiO_2 - ZrO_2$  (ZS). The morphological and physicochemical properties of the catalysts were studied through different characterization techniques and finally, they were evaluated in the HDC of DCF in liquid phase (30 °C, 1 atm, neutral pH) in batch and flow reactors. During these tests, a higher catalytic activity was observed by the  $Al_2O_3$  supported catalysts compared to those supported on ZS due to the larger pore size obtained in the  $Al_2O_3$  supported catalysts and by the presence of a higher amount of sites available for DCF adsorption and activation. Finally, the Pd/ $Al_2O_3$  and Pd-Fe/ $Al_2O_3$ -c catalyst systems showed approximately the same DCF conversion rates both after mild reduction and at high temperature despite the lower Pd<sup>0</sup>/Pd<sup>2+</sup> ratio in the latter catalyst, due to the high PdO reduction capacity in the reaction medium

Wu et al. [14] also prepared Pd catalysts supported on  $Al_2O_3$ , activated carbon (AC),  $SiO_2$ , and  $CeO_2$  using impregnation and precipitation deposition methods. They were evaluated in the HDC of liquid-phase DCF. The characterization results indicated that the Pd/ $CeO_2$  catalyst had a higher Pd dispersion than those supported on  $Al_2O_3$ , AC, and  $SiO_2$ . The binding energy of Pd3d<sub>5/2</sub> in Pd/ $CeO_2$  was higher than that of Pd/ $Al_2O_3$  with a similar Pd loading amount. Furthermore, for Pd/ $CeO_2$  prepared by deposition-precipitation method, the binding energy of Pd3d<sub>5/2</sub> decreased slightly with the loading amount of Pd. As for the catalytic reduction of DCF, Pd/ $SiO_2$  exhibited almost negligible catalytic activity, while the concentration of DCF decreased by 100%, 86% and 29% within 50 min of reaction in Pd/ $CeO_2$ , Pd/ $Al_2O_3$  and Pd/CA, respectively. This fact was indicative of the order of catalytic activity: Pd/ $CeO_2$  > Pd/ $Al_2O_3$  > Pd/CA > Pd/ $SiO_2$ .

On the other hand, Nieto-Sandoval et al., [12] evaluated the commercial Pd/Al<sub>2</sub>O<sub>3</sub> catalyst (1% w/w), achieving complete DCF degradation in 20 min under ambient conditions (25 °C, 1 atm) to [DCF]<sub>0</sub> = 0.068 mM; [Pd/Al<sub>2</sub>O<sub>3</sub>]<sub>0</sub> = 0.5 gL<sup>-1</sup> and H<sub>2</sub> flow of 50 N.mL.min<sup>-1</sup>. It is noteworthy that the chlorinated intermediate (2-(2-chloroanilino)-phenylacetate (Cl-APA)) generated throughout the reaction was completely eliminated at the same time, with the chlorine-free compound 2-anilinophenylacetate (APA) being the only final product. An apparent activation energy of 43 KJ.mol<sup>-1</sup> was obtained, a value comparable to those previously reported for conventional organochlorine contaminants. It is noteworthy that the catalyst exhibited reasonable stability after three successive uses, achieving complete degradation of the drug and obtaining APA as the final product in 30 min.

On the other hand, Zawadzki et al. [15], investigated the catalytic performance of two 1% w/w Pd-loaded BEA zeolites with Si/Al ratio of 19 and 1300 for HDC of DCF. These materials were also studied for comparative purposes with respect to Pd/SiO<sub>2</sub> and Pd/Al<sub>2</sub>O<sub>3</sub> catalyst systems (both at 1% w/w), which are commonly used catalysts in HDC. Regardless of the Si/Al ratio, Pd-loaded BEA catalysts showed 6-fold higher activity than conventional Pd/support catalyst systems. This remarkable performance was mostly attributed to the effect of the three-dimensional structure of the zeolite material.

All the above-mentioned investigations demonstrate the versatility of HDC in the treatment of different matrices contaminated with DCF and which are environmentally subject to study, such as: effluents from wastewater treatment plants and surface waters. However, catalysts that can be obtained from cheaper precursors and that are more stable during the HDC of DCF have not yet been evaluated. From this scenario, in the present investigation, was synthesized zerovalent iron nanoparticles (nZVI) due to their particular characteristics such as low particle size (5-100 nm) [16] and high surface areas, which have allowed them to be efficient materials in remediation processes [16]. In this way, we also intend to evaluate these materials supported on Al<sub>2</sub>O<sub>3</sub> and CA, as potential catalysts for the HDC of DCF in liquid phase. For this purpose, three stages were developed: The synthesis of nZVI from an extract of cypress pine variety *Cupressus Sempervirens*, which is used as a reducing agent due to its phenolic compounds that can transfer electrons to iron ions, forming zerovalent iron nanoparticles [17] and by a reduction method with NaBH<sub>4</sub>; the characterization of these materials by DRX, XPS, Raman Spectroscopy, and TEM and, finally, their catalytic evaluation in the HDC of DCF, for this purpose, the reactions were monitored by HPLC.

## 2 Materials and methods

### 2.1 Synthesis of catalysts (nZVI)

Different catalytic systems were prepared using Fe(NO<sub>3</sub>)<sub>3</sub>.9H<sub>2</sub>O (LOBA Chemie, 98%) as precursor. Likewise, Al<sub>2</sub>O<sub>3</sub> (calcined at 500 °C) and activated carbon (AC) were used for the preparation of the supported catalytic systems. These reagents were used in the procedures described below:

#### 2.1.1 Preparation of cypress pine extract

Cupressus was collected *Sempervirens* in the municipality of Nobsa, Boyacá. Subsequently, the leaves were washed with deionized water and dried for two weeks at room temperature. Then, only the leaflets of each leaf were taken and crushed in an industrial blender to obtain a solid with a smaller particle size. The extract was obtained by a liquid extraction process using 56.7 g of the solid obtained and 250 mL of distilled water, in a reflux equipment at 100 °C until boiling. The mixture was cooled, and the supernatant was separated, which was refrigerated until the synthesis of nZVI-P [18].

#### 2.1.2 Preparation of nZVI-P colloidal systems

The synthesis of zerovalent iron nanoparticles from cypress pine (nZVI-P) was carried out from a 1.0 M solution of Fe(NO<sub>3</sub>)<sub>3</sub>.9H<sub>2</sub>O. The cypress pine extract was placed in a burette and allowed to drip onto the precursor solution (previously placed in a beaker), which was kept at 30 °C with stirring at 3000 rpm. The reaction process was maintained for 20 hours.

#### 2.1.3 Preparation of nZVI-A colloidal systems

Sodium borohydride-reduced zerovalent iron nanoparticles (nZVI-A) were prepared from a 0.5 M solution of Fe(NO<sub>3</sub>)<sub>3</sub>.9H<sub>2</sub>O and a 2.0 M solution of NaBH<sub>4</sub> (98% Aldrich). The ferric nitrate solution was added in a side-sealed flask sealed with a stopper, while the borohydride solution was placed in a burette. Thus, the borohydride solution was slowly added to the ferric nitrate solution. The reaction system was maintained at 35 °C and stirred at 180 rpm. In addition, the hydrogen produced during the reaction was captured by bubbling in water contained in a flask. After the reaction process was finished, the mixture was kept stirring for 10 minutes. The precipitate obtained was filtered using a vacuum pump (102 Moderate filter paper of 125 nm was used) and its pH was adjusted to 7.0 by progressive washing with distilled water. Finally, the solid called nZVI-A was obtained, which was dried for 12 hours in a Heat oven. eLDS at 130 °C, using a heating ramp of 3.6 °C/min.

#### 2.1.4 Preparation of supported catalyst systems nZVI-A/CA, nZVI-P/CA and nZVI-P/Al<sub>2</sub>O<sub>3</sub>

Colloidal iron nanoparticles were impregnated in activated carbon and alumina at a metal loading of 15% nZVI by mass and subsequently dried at 350 °C and passivated for 15 minutes using constant N<sub>2</sub> pumping, in a closed system. In this way, the catalysts nZVI-P/Al<sub>2</sub>O<sub>3</sub> and nZVI-P/CA were obtained. The activated carbon used as support was obtained from soursop seed, by maceration-impregnation method of MgCl<sub>2</sub> at 5% w/v under carbonization conditions at 800 °C and washed until constant pH. Finally, all the catalysts obtained were stored and refrigerated until their subsequent use in the characterization stage.

## 2.2 Characterization of catalysts

### 2.2.1 X-ray diffraction (XRD)

This technique was used to determine the different crystalline phases present in the synthesized catalysts. X-ray

diffractograms were obtained using a diffractometer Rigaku miniflex with Cu K $\alpha$  radiation ( $\lambda = 0.1518$  nm). The analysis conditions were: 40 mV and 20 mA with Bragg angles between 5° and 90°, using continuous scanning with a step of 0.02°/min in  $2\theta$ . All diffractograms were processed using X'Pert software HighScore Plus. The main diffraction peaks were indexed using different crystallographic charts.

### 2.2.2 X-ray photoelectron spectroscopy (XPS)

The oxidation states of the chemical species present in the catalysts obtained were determined. These analyses were carried out in a Thermo Scientific spectrometer. Scientific model Escalab 250 Xi with monochromatic Al K $\alpha$  radiation (1486.6 eV) and a pressure of  $1 \times 10^{-9}$  mbar. The equipment was operated with a constant energy step of 25 eV and a step size of 0.05 eV and Ar<sup>+</sup> etching was used for all analyses using an ion energy of 1000 eV, an etching time of 30 s, and a medium current. In all experiments, the C 1s signal (284.6 eV) was used as reference and measurements were performed at room temperature. CasaXPS software was used to process the obtained spectra.

### 2.2.3 Transmission Electron Microscopy (TEM)

This analysis was developed to determinate the average particle size and particle size distributions in each of the prepared catalytic materials. For this purpose, the catalysts were pretreated by dispersion in isopropyl alcohol and ultrasonicated for 1.5 hours at room temperature before analysis. Subsequently, bright field TEM micrographs were obtained at 10 nm, 20 nm, 50 nm, 100 nm, 200 nm and 500 nm, using a FETEM microscope, JEOL Model JEM-2100F with an acceleration voltage of 200 kV. The average particle size was calculated by counting 200 particles from the TEM micrographs, which were previously processed in Image J software.

Additionally, the percentage of dispersion (%D) of the nZVI on the Al<sub>2</sub>O<sub>3</sub> and CA was determined (Eq. 1), assuming that the metallic particles were dispersed in a homogeneous circular shape. Finally, particle size distribution histograms were obtained for each catalyst.

$$\%D = \frac{1}{d} * 100 \quad (1)$$

### 2.2.4 Raman Spectroscopy

The Raman Spectroscopy technique was carried out to verify the chemical nature of the synthesized catalysts according to their main vibrational modes. The analyses were performed at room temperature in a confocal microscope Raman (Witec, alpha 300), using a green Nd-YAG laser (with a wavelength of 532 nm) and a 50 $\times$  objective lens. 400 scans were used to obtain the Raman spectra of each sample.

### 2.3 Catalytic evaluation

The DCF-HDC reactions were carried out in liquid phase at room temperature using a 250 mL three-necked flask. Additionally, the whole process was carried out under a constant flow of H<sub>2</sub> (30 mL/min). Each reaction was carried out starting

from 70 mL of 0.025 mM Diclofenac sodium salt solution and using 0.5 g of catalyst. Additionally, the stirring speed of the reaction system was maintained at 300 rpm. During each test, periodic samples were taken until 360 minutes of reaction, and were subsequently filtered and injected in a HPLC equipment (Agilent 1200 Infinity), with a UV detector 1100 Azura and a C18 type column ZORBAX Eclipse XDR-C18 (Analytical 4.6  $\times$  150mm  $\times$  5-Micron). 20  $\mu$ L of each sample were injected, which previously were filtered (0.45  $\mu$ m membrane filters), using an injection temperature of 30 °C,  $\lambda = 245$  nm, mobile phase (MP) of water/methanol/acetonitrile (50:23:27) and a MP flow of 0.4 mL/min. From the chromatograms obtained, the DCF conversion parameters (XDCF), selectivity to APA (SAPA) and selectivity to CI-APA (SCI-APA) were determined. For this purpose, the equations (Eq. 2, Eq. 3 and Eq. 4) shown below were taken into account:

$$X_{DFC}(\%) = \frac{\text{Mols DFC}_{initial} - \text{Mols DFC}_{final}}{\text{Mols DFC}_{initial} * 100} \quad (2)$$

$$S_{APA}(\%) = \frac{(\text{Mols APA})}{(\text{Total Mols of products}) * 100} \quad (3)$$

$$S_{(CI-APA)}(\%) = \frac{\text{Mols CI} - \text{APA}}{(\text{Total Mols of product}) * 100} \quad (4)$$

## 3 Results and discussion

### 3.1 Characterization of catalysts

#### 3.1.1 X-ray diffraction (XRD)

Figure 2 shows the X-ray diffraction patterns of nZVI-A/CA, nZVI-P/CA, nZVI-P/Al<sub>2</sub>O<sub>3</sub> and nZVI-P. The nZVI-P system exhibited peaks at  $2\theta = 43.3^\circ$  and  $64.4^\circ$ , which were attributed to the (110) and (200) planes of Fe 0 (JCPDS 65-4899) with a BCC (body-centered cubic) structure. Pine contains cellulose and its essential oil, corresponding to the cypress pine extract used, in its leaflets. Thus, it can be suggested that only the large pores of the structure are occupied at low concentrations. The diffraction pattern of unmodified pine has diffraction peaks at 15°, 17° and 22°, which are derived from cellulose [19]. Likewise, other signals that were observed indicated the presence of iron oxy-hydroxide (FeOOH, BCC structure) towards  $2\theta = 21.3^\circ$ , and organic matter towards  $2\theta = 25.03^\circ$ . This signal suggests the presence of organic matter, may be subject to the presence of different chemical species such as  $\alpha$ -pinene and  $\beta$ -pinene, borneol, limonene, terpinene, ocimene, myrcene, sabinene and alpha-terpinene that would act as stabilizing agents of the iron particles [20].

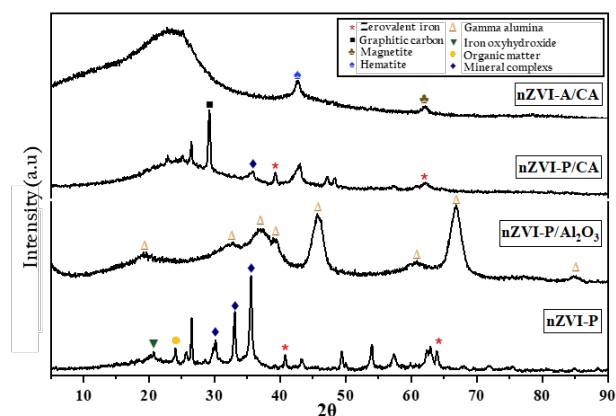


Figure 2: X-ray diffraction patterns of nZVI-A/CA, nZVI-P/CA, nZVI-P/Al<sub>2</sub>O<sub>3</sub> and nZVI-P.

The nZVI-P/CA catalyst showed signals at  $2\theta = 29.8^\circ$ ,  $33.1^\circ$  and  $35.5^\circ$  are attributed to the presence of mineral complexes contained in the cypress pine, such as those mentioned above for the nZVI-P/CA catalytic system [18]. Likewise, the presence of crystalline structures of graphitic carbon at the level of the catalytic support was verified, by observing the peaks at  $2\theta = 29.08^\circ$  indexed to the (101) plane (JCPDS 41-1487, which is attributed to the crystalline turbostratic structure that follows an alignment of disordered layers of graphitic carbon. On the other hand, the diffraction peak at  $36.02^\circ$  was related to the presence of mineral complexes. This is suggested because studies have been carried out on the synthesis of ultrafine particles and nanoparticles of pine and its bark in specimens such as *Pinus Patula* and *Pinus Radiata*, which bear a great resemblance to the *Cupressus pine Sempervirens*, where it is mentioned that pine in its different varieties contains mainly mineral complexes of calcium, magnesium, potassium and phosphorus, in addition to elements such as iron, magnesium and zinc [21]. While the signals observed towards  $2\theta = 43.3^\circ$  and  $64.4^\circ$  were related to the (110) and (200) planes of Fe 0 (JCPDS 65- 4899) with BCC structure [22].

On the other hand, the nZVI-P/Al<sub>2</sub>O<sub>3</sub> system only showed reflections related to the catalytic support ( $\gamma$ -Al<sub>2</sub>O<sub>3</sub>). Thus, no signals attributed to the characteristic reflections for iron species were detected and, in this case, only signals attributed to the ( $\gamma$ -Al<sub>2</sub>O<sub>3</sub>) phase of the support were detected. The absence of Fe 0 signals can be related to the high distribution of nanoparticles supported on alumina, since this material has thermal stability and a high surface area [23]. The characteristic peaks for  $\gamma$ -Al<sub>2</sub>O<sub>3</sub> were observed at diffraction angles of  $19.2^\circ$  (111),  $32.3^\circ$  (220),  $37^\circ$  (311),  $39.2^\circ$  (222),  $46^\circ$  (400),  $60.6^\circ$  (333),  $66.7^\circ$  (440),  $85^\circ$  (444) (JCPDS 29-0063) [24].

According to the diffractograms shown in Figure 6, the nZVI-A/CA system exhibited diffraction peaks that suggested a mixture of two phases corresponding to hematite ( $\alpha$ -Fe<sub>2</sub>O<sub>3</sub>), for which a small signal is observed towards  $2\theta \approx 42.8^\circ$ , and magnetite (Fe<sub>3</sub>O<sub>4</sub>), showing a signal at  $2\theta \approx 64.8^\circ$ . This could be corroborated by comparing the signals obtained in these XRD patterns with those obtained in the studies of Bertolucci et al., in which similar diffractions are also detected for this type of crystalline phases, suggesting the presence

of a magnetite phase (Fe<sub>3</sub>O<sub>4</sub>) and another phase of hematite ( $\alpha$ -Fe<sub>2</sub>O<sub>3</sub>) [25].

### 3.2 X-ray photoelectron spectroscopy (XPS)

Figure 3 shows the XPS spectra obtained for the synthesized catalysts. The XPS spectra for the analyzed catalytic systems present signals corresponding to the Fe 2p region, where peaks that reflect the binding energy are observed, according to characteristic signals. An intense peak at 706.90 eV is evident in the nZVI-P catalytic system, which is attributed to the Fe 2p<sub>3/2</sub> state of metallic iron (Fe<sup>0</sup>). The peaks of oxidized iron species (Fe<sup>2+</sup> and Fe<sup>3+</sup>) are attributed to the presence of iron oxyhydroxide (FeOOH) and iron hydroxides (Fe(OH)<sub>x</sub>), which can be detected by XRD, which suggests the formation of amorphous structures of iron hydroxides during the passivation step of the catalytic materials, according to Liang et al. [26].

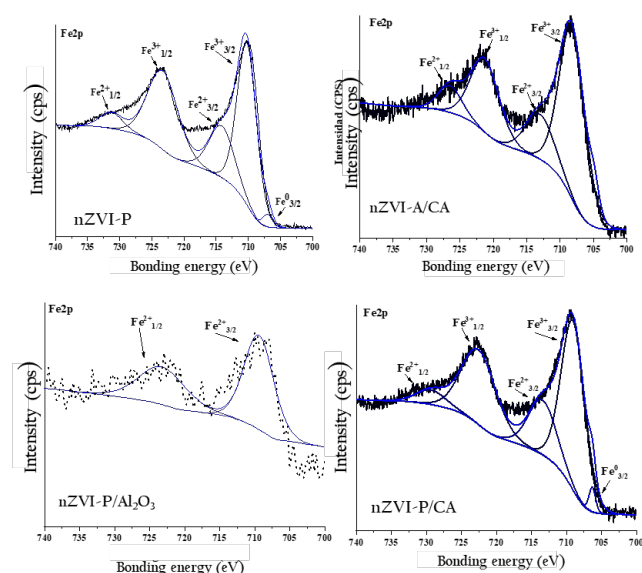


Figure 3: XPS spectrum in the Fe2p state for the catalytic systems.

The nZVI-A/CA catalyst exhibited the signal of the Fe2p<sub>3/2</sub> state of iron in its oxidized species Fe<sup>2+</sup> was found in the XPS spectrum, which are predominant at the surface level in this catalyst. The absence of signals related to the presence of Fe<sup>0</sup>, suggests that oxidation of the catalyst may have occurred, because other species with similar doublets were present that are related to the presence of iron oxide type species. In the same way, the XPS spectrum obtained for the nZVI-P/Al<sub>2</sub>O<sub>3</sub> catalytic system, two signals corresponding to the Fe 2p<sub>1/2</sub> and Fe2p<sub>3/2</sub> states were observed, which are attributed to the iron oxidation state Fe<sup>3+</sup> [26]. By observing the XPS spectrum obtained for the nZVI-P/CA catalytic system, and comparing it with the XRD pattern obtained for this same catalyst, the presence of zerovalent iron could be confirmed. This could be verified by observing a small signal near 704.35 eV corresponding to the zerovalent iron binding energy 2p<sub>3/2</sub> [27].

### 3.3 Transmission Electron Microscopy (TEM)

The TEM micrographs are presented in Figure 4 with their respective particle size distribution histograms. It can be seen that the materials have spherical and irregular shapes with heterogeneous particle size distribution. Table 1 shows the average particle sizes, where a particle size mostly between 3.4 nm and 6.0 nm was found. For the nZVI-P system, an average particle size of 6.0 nm was obtained, whereas the nZVI-P/CA and nZVI-P/Al<sub>2</sub>O<sub>3</sub> catalysts exhibited an average particle size of 3.4 nm and 4.5 nm, respectively. This behavior confirms the relevance of supports in the distribution and dispersion of particles, inducing small particle sizes [28]. In the same way, the nZVI-A/CA system, showed a similar average particle size (4.7 nm) nZVI-P/Al<sub>2</sub>O<sub>3</sub>, but the distribution of particle sizes was much higher, reaching sizes between 1 and 14 nm. Table 1 shows the dispersion of catalysts from TEM analysis. nZVI-A/CA exhibited the lowest percentage of dispersion, while the nZVI-P/CA catalysts presented the highest dispersion, which can be related with the preparation method, being the green syntheses from pine favors the low particle size when the particles are supported. It is important to note that the particle size in a catalytic system can have an impact on the activity and selectivity of the catalysts.

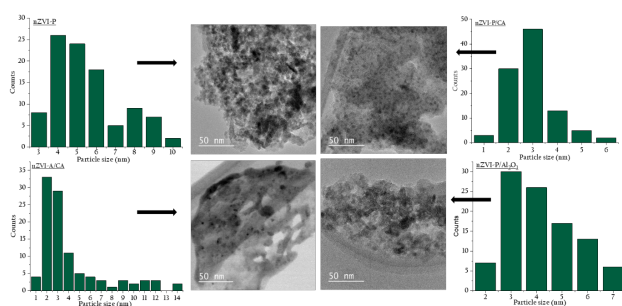


Figure 4: Typical TEM images and particle size distribution of nanoparticles of zerovalent iron (nZVI) and nZVI supported.

Table 1. Average particle sizes (d) and dispersion percentages (%D) obtained for the synthesized catalysts.

Catalyst	d(nm)	%D*
nZVI-A/CA	4.7	21
nZVI-P/CA	3.4	29
nZVI-P/Al <sub>2</sub> O <sub>3</sub>	4.5	22
nZVI-P	6.0	-

\* Calculate by TEM.

### 3.4 Raman Spectroscopy

The Raman spectroscopy analysis allows determination of the presence of other Fe ionic species present in the synthesized materials and the nature of the carbon present at the support level and could be verified, by measuring the energy change between the incident and scattered photons, which are associated with the Stokes and Anti-Stokes transitions [29, 30].

In the Raman spectrum of the nZVI-P catalyst (Figure 5), signals were observed at 222 cm<sup>-1</sup>, 289 cm<sup>-1</sup> and 400 cm<sup>-1</sup> attributed to three vibrational modes of hematite (Space Group R-3c according to Hermann-Mauguin notation, with the modes 2A<sub>1g</sub> + 4E<sub>g</sub>, expected by group theory). These

nanoparticles obtained from natural pine extracts can contain a wide range of contaminants due to their large surface area and redox potential. The signal that appears at 1500 cm<sup>-1</sup> in Raman spectroscopy may refer to a stretching or bending vibrational mode of some functional group or of some part of the molecular structure of the nZVI system or the pine extract. Some examples of functional groups that can be absorbed in this region are carbonyl (C=O), nitrile (C≡N), nitro (NO<sub>2</sub>), alkene (C=C), aromatic (C=C), among others. The exact position and intensity of the signal depend on the nature of the bond, the strength of the incident electric field, the molecular environment, and the symmetry of the vibrational mode [31].

As for the CA-supported systems (nZVI-P/CA and nZVI-A/CA), the signals at 1360 cm<sup>-1</sup> and 1600 cm<sup>-1</sup> were observed, related to the D and G bands (C-C bond stretching) respectively. The presence of these bands allowed to verify that both synthesized systems present a mixture of disordered graphitic carbon (D) and properly graphitized carbon (G) crystalline structures [32]. The nZVI-P/CA system also presented a band close to 400 cm<sup>-1</sup> attributed to vibrational modes Eg. This set of signals corresponds with the Raman bands expected for hematite (α-Fe<sub>2</sub>O<sub>3</sub>, with crystal space group D 6 3h) based on point group theory (2A<sub>1g</sub> + 4E<sub>g</sub>), and is consistent with those reported in previous studies [31, 32].

On the other hand, the nZVI-P/Al<sub>2</sub>O<sub>3</sub> system did not exhibit bands attributed to metal oxide vibrations (like that of hematite), with only small non-representative signals attributed to detector noise. Studies have been performed on γ-Al<sub>2</sub>O<sub>3</sub> models. The spinel primitive cell of this alumina contains 40 atoms in the unit cell and has 57 Raman active modes (34 Ag and 23 Bg) and 60 IR active modes (25 Au and 35 Bu). On the other hand, the non-spinel γ-Al<sub>2</sub>O<sub>3</sub> primitive cell has 60 Raman active modes (34 Ag and 26 Bg), according to Liu, et al [34].

For this phase of alumina, unfortunately, no experimental vibration mode assignments have been found available. The dispersion of alumina prevents the determination of the vibrational modes because alumina is a very dispersed material and a clear signal of the vibrational modes cannot be obtained [35]. This can be correlated with the noise found in the XPS spectrum. Therefore, it is attributed that in the nZVI-P/Al<sub>2</sub>O<sub>3</sub> system only the presence of the support is found, as found in the XRD diffractogram, where only reflections related to the catalytic support (γ-Al<sub>2</sub>O<sub>3</sub>) were found [34].

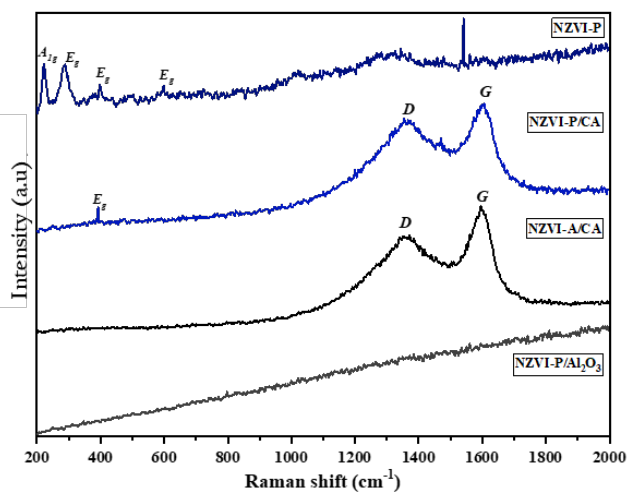


Figure 5: Raman spectra for nZVI-P, nZVI-P/CA, nZVI-A/CA and nZVI-P/Al<sub>2</sub>O<sub>3</sub> catalysts.

#### 4 Catalytic evaluation

The performance of the nZVI-P catalyst supported on Al<sub>2</sub>O<sub>3</sub> and CA and nZVI-A supported on CA in the hydrodechlorination reaction of diclofenac to obtain 2-anilinophenylacetate was evaluated. Figure 6 shows the conversion of DCF in the different catalytic systems over the 360 minutes of reaction. It was observed that the conversion increased with reaction time. In the first hour of reaction (60 min), it was observed that the nZVI-P and nZVI-P/CA catalysts showed a similar conversion. However, in the next sampling, the supported catalyst increased by almost 20% compared to the unsupported one. This suggests that activated carbon, due to its high adsorption capacity, inertness and chemical stability, as well as its versatile surface chemistry and mechanical strength, together with the iron present in the catalyst, enhances the adsorption of negatively charged contaminants, in this case, Cl<sup>-</sup> ions, resulting in increased DCF conversion.[36, 37]

The nZVI-P/CA catalyst achieved a conversion higher than 90% at 360 minutes of reaction, while the dispersion in the trend line increased during the different reaction times. The nZVI-A/CA catalyst, despite having the same support, obtains a lower conversion percentage, around 40%. This may be related to the absence of Fe<sup>0</sup> signals in the XPS spectra. In addition, the catalyst supported on alumina showed a high conversion at the beginning of the reaction, but experienced a deactivation over time, remaining at values close to 80%. This is attributed to a lower dispersion of the metal in the support, which is observed in the transmission electron microscopy analysis, and to a larger particle size, which contributes to maintaining a constant conversion of diclofenac, highlighting that according to the XPS analysis, no Fe<sup>0</sup> signals were presented. The unsupported nZVI-P catalyst showed an intermediate conversion of 60%, suggesting that the support plays an important role in the mechanical stability of the catalyst. Supports immobilize the particles, reducing their mobility and favoring their chemical stabilization [38].

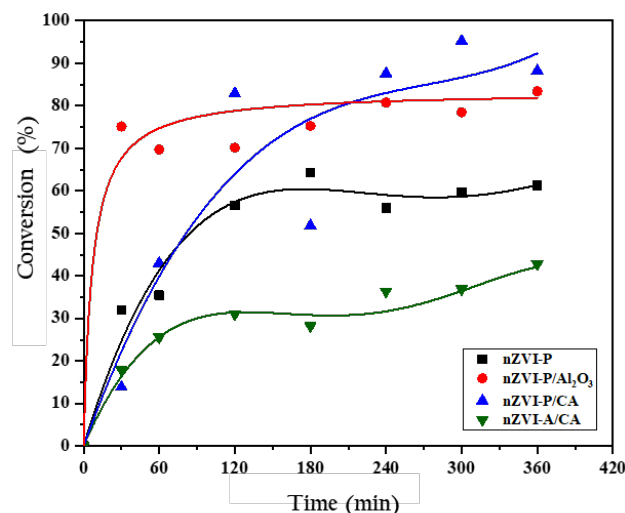


Figure 6: DFC conversion on nZVI-P, nZVI-P/Al<sub>2</sub>O<sub>3</sub>, nZVI-P/CA and nZVI-A/CA. Reaction conditions: [DFC]<sub>0</sub>: 0.025 mM; catalyst mass: 0.5 g; 30 °C.

Regarding the selectivity towards the formation of the intermediate and final reaction products (2-(2-chloroanilino)-phenylacetate (CI-APA) and 2-anilinophenylacetate (APA)) shown in Figure 7, it was found that the highest percentage of selectivity for CI-APA was reached at 300 minutes of reaction using the nZVI-P/Al<sub>2</sub>O<sub>3</sub> catalyst, with a selectivity percentage higher than 4%. This catalyst showed the best selectivity at the rest of the reaction times, although none exceeded 3%. On the other hand, the nZVI-P/CA catalyst showed the lowest selectivity at the other reaction times. The other two catalysts, nZVI-P and nZVI-A, also obtained low selectivity, occupying third and fourth place respectively in the average of the time measurements.

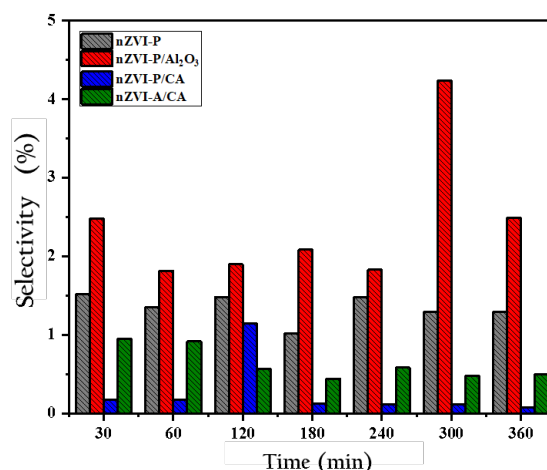


Figure 7: Cl-APA selectivity during HDC of DFC on nZVI-P; nZVI-P/Al<sub>2</sub>O<sub>3</sub>, nZVI-A/CA and nZVI-A/CA. Reaction conditions: [DFC]<sub>0</sub>: 0.025 mM; catalyst mass: 0.5 g; 30 °C.

Regarding the APA product is the product of interest, it was observed that the nZVI-P/CA catalyst showed the highest

selectivity, reaching a value close to 100% at 360 minutes of reaction, and maintaining a similar selectivity at the other times (Figure 8). On the other hand, the nZVI-P/Al<sub>2</sub>O<sub>3</sub> catalyst exhibited the lowest selectivity at all reaction times, and its lowest percentage was recorded at 300 minutes, where it had obtained the best selectivity for the CI-APA product, as indicated in Figure 8. This suggests that the catalysts preferentially carry out the dechlorination of the two Cl atoms of diclofenac, generating high production of APA. Since the selectivity of a catalyst is related to its ability to direct the reaction in a preferential direction, it can be inferred that during the reaction there was a change in the preferred selectivity towards one or another reaction product. It is important to note that the selectivity of the catalyst is higher when a higher concentration of the desired product is obtained compared to the total possible products, and this was variable in both products obtained. A similar behavior was observed by Lokteva et al., [39] to study the effect of iron content in alumina-supported palladium catalysts and their reduction conditions on diclofenac hydrodechlorination in an aqueous medium.

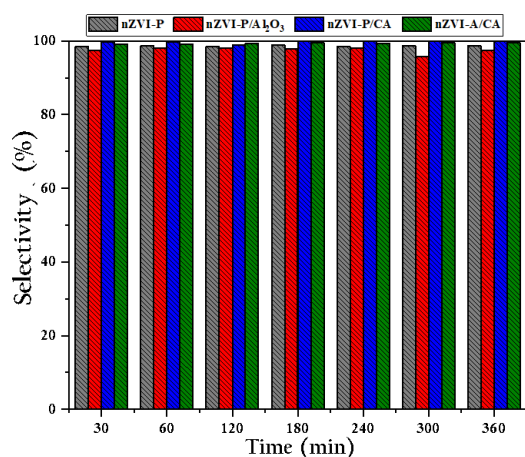


Figure 8: APA selectivity during HDC of DFC on nZVI-P; nZVI-P/Al<sub>2</sub>O<sub>3</sub>; nZVI-A/CA. Reaction conditions: [DFC]<sub>0</sub>: 0.025 mM; catalyst mass: 0.5 g; 30 °C.

Figure 9 shows the behavior of the products obtained during the HDC of DCF using nZVI-A/CA as an example. It can be deduced that this has a consecutive reaction behavior since a gradual increase in the obtaining of APA is observed throughout the reaction time, while the concentration of CI-APA reaches its maximum value at the beginning of the reaction and then decreases as the reaction time progresses. Therefore, if the CI-APA product was formed faster than the APA during the reaction, it is established that it is due to the nature of the reaction and/or the number of reacting species [14]. Thus supporting that the greater the catalyst activity, the presence of zerovalent iron can be determined, when evaluating the catalytic activity in the HDC, which refers to the capacity of each catalyst to promote the reaction, nZVI-P/CA stands out as the most active, and at the same time maintains a high selectivity towards APA, making it a promising option to complement the method of transformation of the organochlorine compound.

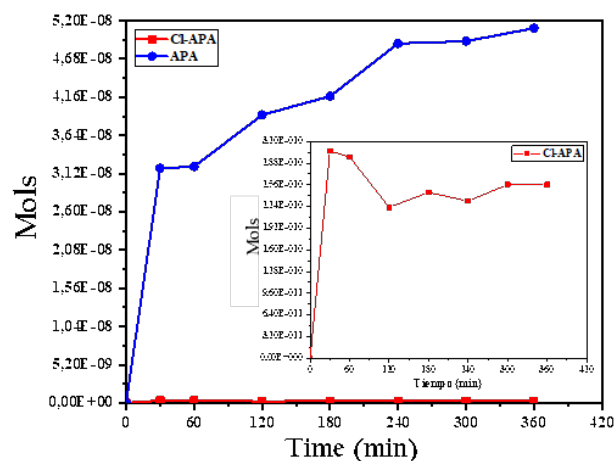


Figure 9: Products obtained during the HDC of DFC on nZVI-A/CA. Reaction conditions: [DFC]<sub>0</sub>: 0.025 mM; catalyst mass: 0.5 g; 30 °C.

## 5 Conclusions

HDC with supported and unsupported nZVI is a promising model process for the treatment of water sources contaminated by COC. This is attributed to the high catalytic capacity exhibited by these systems during the HDC of DCF, leading to the generation of less toxic compounds.

The use of Raman spectroscopy has allowed to identify the oxide species present in the catalysts and to characterize the D and G bands of the carbon used as support. In the case of the nZVI-P catalyst, signals attributed to vibrational modes of hematite were observed, indicating the presence of iron nanoparticles in the material. The systems supported on CA (nZVI-P/CA and nZVI-A/CA) showed signals related to the D and G bands, suggesting a mixture of disordered graphitic carbon and graphitic carbon crystal structures.

It was observed that the diclofenac conversion increased with reaction time in all catalytic systems. The nZVI-P/CA catalyst achieved a high conversion close to 100%. On the other hand, the nZVI-A/CA catalyst, despite having the same support, presented a lower conversion of around 40%. The catalyst supported on alumina showed a high initial conversion, but experienced a deactivation throughout the reaction, remaining at values close to 80%. The low particle size, the presence of metallic iron and the use of carbon as support played an important and favorable role in the conversion of the catalysts.

Regarding the selectivity towards the reaction products, all catalysts showed high levels of selectivity towards the product of interest APA. CI-APA was present in small quantities, being an intermediate of the hydrodechlorination reaction of diclofenac.

## Acknowledgments

The authors acknowledge the financial support provided by the Vicerrectoría de Investigación y Extensión–Universidad Pedagógica y Tecnológica de Colombia by the project SGI 3567 and RECAT-UFF to characterization analysis.

### Author Contributions

All authors contributed to the study conception and design. Material preparation, data collection and analysis were performed by Luna López, Paula Ramirez and Maria H. Brijaldo. The first draft of the manuscript was written by Luna López and all authors commented on previous versions of the manuscript. All authors read and approved the final manuscript. Funding: This research was funded by the Vicerrectoría de Investigación y Extensión–Universidad Pedagógica y Tecnológica de Colombia by the project SGI 3567.

### References

- [1] J. N. Malagón-Rojas, C. F. Garrote-Wilches, y M. Varona, "A debt from the past: effects of organochlorines on workers in the vector control program - Colombia," *Journal of the Industrial University of Santander. Health*, vol. 46, no. 3, pp. 227–235, 2014. [Online]. Available: [http://www.scielo.org.co/scielo.php?script=sci\\_arttext&pid=S0121-08072014000300003&lng=en&nrm=iso&tlng=es](http://www.scielo.org.co/scielo.php?script=sci_arttext&pid=S0121-08072014000300003&lng=en&nrm=iso&tlng=es)
- [2] J. N. Malagón Rojas, C. F. Garrote Wilches, y M. Varona, "Una deuda del pasado: efectos de los organoclorados en trabajadores del programa de control de vectores - Colombia," *Rev. Univ. Ind. Santander. Salud*, vol. 46, no. 3, pp. 227–235, Oct. 2014.
- [3] T. O. Ajiboye, A. T. Kuvarega, y D. C. Onwudiwe, "Recent strategies for environmental remediation of organochlorine pesticides," *Applied Sciences (Switzerland)*, vol. 10, no. 18, Sep. 2020, doi: 10.3390/APP10186286.
- [4] O. M. L. Alharbi, A. A. Basheer, R. A. Khatlab, y I. Ali, "Health and environmental effects of persistent organic pollutants," *J. Mol. Liq.*, vol. 263, pp. 442–453, Aug. 2018, doi: 10.1016/J.MOLLIQ.2018.05.029.
- [5] M. Parolini, "Toxicity of the Non-Steroidal Anti-Inflammatory Drugs (NSAIDs) acetylsalicylic acid, paracetamol, diclofenac, ibuprofen and naproxen towards freshwater invertebrates: A review," *Sci. Total Environ.*, vol. 740, Oct. 2020, doi: 10.1016/J.SCITOTENV.2020.140043.
- [6] G. I. Tovar-Aguilar, M. A. Arzate-Cardenas, y R. Rico-Martínez, "Effects of diclofenac on the freshwater rotifer *Lecane papuana* (Murray, 1913) (Monogononta: Lecanidae)," *Hidrobiológica*, vol. 29, no. 2, Mar. 2021. [Online]. Available: [https://www.scielo.org.mx/scielo.php?script=sci\\_arttext&pid=S0188-88972019000200063](https://www.scielo.org.mx/scielo.php?script=sci_arttext&pid=S0188-88972019000200063)
- [7] S. De Wildeman, G. Diekert, H. Van Langenhove, y W. Verstraete, "Stereoselective microbial dehalorespiration with vicinal dichlorinated alkanes," *Appl. Environ. Microbiol.*, vol. 69, no. 9, pp. 5643–5647, Sep. 2003, doi: 10.1128/AEM.69.9.5643-5647.2003.
- [8] S. Chong, G. Zhang, N. Zhang, Y. Liu, T. Huang, H. Chang, "Diclofenac degradation in water by FeCeOx catalyzed H<sub>2</sub>O<sub>2</sub>: Influencing factors, mechanism and pathways," *J. Hazard. Mater.*, vol. 334, pp. 150–159, Jul. 2017, doi: 10.1016/j.jhazmat.2017.04.008.
- [9] V. Muelas-Ramos, M.J. Sampaio, C.G. Silva, J. Bedia, J.J. Rodriguez, J.L. Faria, C. Belver, "Degradation of diclofenac in water under LED irradiation using combined g-C<sub>3</sub>N<sub>4</sub>/NH<sub>2</sub>-MIL-125 photocatalysts," *J. Hazard. Mater.*, vol. 416, p. 126199, Aug. 2021, doi: 10.1016/J.JHAZMAT.2021.126199.
- [10] J.E. Casillas, F. Tzompantzi, Guadalupe Gregorio Carbajal-Arizaga, J. Aguilar-Martínez, V.V.A. Fernández-Escamilla, Esthela Ramos-Ramírez, Miguel Angel López-Álvarez, C. Tzompantzi-Flores, A. Barrera, "Coupled Al-Ga-xAg composites prepared by the sol-gel method and their efficient photocatalytic performance in the degradation of diclofenac," *Surfaces and Interfaces*, vol. 30, p. 101809, Jun. 2022, doi: 10.1016/J.SURFIN.2022.101809.
- [11] M. Munoz, Z. M. de Pedro, J. A. Casas, y J. J. Rodriguez, "Improved  $\gamma$ -alumina-supported Pd and Rh catalysts for hydrodechlorination of chlorophenols," *Appl. Catal. A Gen.*, vol. 488, pp. 78–85, Nov. 2014, doi: 10.1016/J.APCATA.2014.09.035.
- [12] J. Nieto-Sandoval, M. Munoz, Z. M. de Pedro, y J. A. Casas, "Fast degradation of diclofenac by catalytic hydrodechlorination," *Chemosphere*, vol. 213, pp. 141–148, Dec. 2018, doi: 10.1016/j.chemosphere.2018.09.024.
- [13] E.S. Lokteva, V.V. Shishova, K.I. Maslakov, E.V. Golubina, A.N. Kharlanov, I.A. Rodin, M.F. Vokuev, D.S. Filimonov, N.N. Tolkachev, "Bimetallic PdFe catalysts in hydrodechlorination of diclofenac: Influence of support nature, metal deposition sequence and reduction conditions," *Appl. Surf. Sci.*, vol. 613, Mar. 2023, doi: 10.1016/J.APSUSC.2022.156022.
- [14] K. Wu, X. Qian, L. Chen, Z. Xu, S. Zheng y D.Zhu., "Effective liquid phase hydrodechlorination of diclofenac catalyzed by Pd/CeO<sub>2</sub>," *RSC Adv.*, vol. 5, no. 24, pp. 18702–18709, Feb. 2015, doi: 10.1039/C4RA16674D.
- [15] Y. Long, J. Liang, y Y. Xue, "Ultrasound-assisted electrodeposition synthesis of nZVI-Pd/AC toward reductive degradation of methylene blue," *Environ. Sci. Pollut. Res. Int.*, vol. 28, no. 47, pp. 67098–67107, Dec. 2021, doi: 10.1007/S11356-021-15316-0.
- [16] Y. B. Hu y X. Y. Li, "Influence of a thin aluminum hydroxide coating layer on the suspension stability and reductive reactivity of nanoscale zero-valent iron," *Appl. Catal. B*, vol. 226, pp. 554–564, Jun. 2018, doi: 10.1016/J.APCATB.2017.12.077.
- [17] M. Rosales Castro y R. F. González Laredo, "Comparison of the content of phenolic compounds in the bark of eight pine species," *Madera y Bosques*, vol. 9, no. 2, pp. 41–49, 2003. [Online]. Available: <https://www.redalyc.org/pdf/617/61790204.pdf>
- [18] A. Ebrahiminezhad, S. Taghizadeh, Y. Ghasemi, A. Berenjian, "Green synthesized nanoclusters of ultra-small zero valent iron nanoparticles as a novel dye removing material," *Sci. Total Environ.*, vol. 621, pp. 1527–1532, Apr. 2018, doi: 10.1016/J.SCITOTENV.2017.10.076.
- [19] N. A. Soto, W. R. Machado, y D. L. López, "Determination of kinetic parameters in the pyrolysis of cypress

- pine," *Quim. Nova*, vol. 33, no. 7, pp. 1500–1505, 2010, doi: 10.1590/S0100-40422010000700014.
- [20] M. Fazlzadeh, K. Rahmani, A. Zarei, H. Abdoallahzadeh, F. Nasiri, y R. Khosravi, "A novel green synthesis of zero valent iron nanoparticles (NZVI) using three plant extracts and their efficient application for removal of Cr(VI) from aqueous solutions," *Advanced Powder Technology*, vol. 28, no. 1, pp. 122–130, 2017, doi: 10.1016/j.appt.2016.09.003.
- [21] P. Santodomingo G., "Synthesis of ultrafine particles and nanoparticles from pine bark (*Pinus patula*) for the removal of hexavalent chromium (Cr (VI)) in contaminated waters," Universidad de Los Andes, 2018. [Online]. Available: <https://repositorio.uniandes.edu.co/bitstream/handle/1992/39189/u821069.pdf?sequence=1>
- [22] M. M. El-Shafei & A. Hamdy, "Zero-valent iron nanostructures: synthesis, characterization and application," *J. Environ. Biotechnol. Res.*, vol. 7, no. 1, pp. 1–10, 2018. [Online]. Available: [www.vinanie.com/jebr](http://www.vinanie.com/jebr)
- [23] V. P. Pakharukova, D. A. Yatsenko, E. Y. Gerasimov, A. S. Shalygin, O. N. Martyanov, y S. V. Tsybulya, "Coherent 3D nanostructure of  $\gamma$ -Al<sub>2</sub>O<sub>3</sub>: Simulation of whole X-ray powder diffraction pattern," *Journal of Solid State Chemistry*, vol. 246, pp. 284–292, 2017, doi: 10.1016/j.jssc.2016.11.032.
- [24] G. Sun, X. Mu, Y. Zhang, Y. Cui, G. Xia, Z. Chen, "Rare earth metal modified CuO/ $\gamma$ -Al<sub>2</sub>O<sub>3</sub> catalysts in the CO oxidation," *Catal. Commun.*, vol. 12, no. 5, pp. 349–352, Jan. 2011, doi: 10.1016/j.CATCOM.2010.10.013.
- [25] S. A. Messele, C. Bengoa, F. Stüber, A. Fortuny, A. Fabregat, J. Font, "Catalytic wet peroxide oxidation of phenol using nanoscale zero-valent iron supported on activated carbon," *Desalination Water Treat.*, vol. 57, no. 11, pp. 5155–5164, Mar. 2015, doi: 10.1080/19443994.2014.1002011.
- [26] W. Liang, C. Dai, X. Zhou, y Y. Zhang, "Application of Zero-Valent Iron Nanoparticles for the Removal of Aqueous Zinc Ions under Various Experimental Conditions," *PLOS ONE*, vol. 9, no. 1, p. e85686, 2014, doi: 10.1371/journal.pone.0085686.
- [27] C. Wang, Z. Xu, G. Ding, X. Wang, M. Zhao, S. Sai Hang & Yunchun Li., "Comprehensive study on the removal of chromate from aqueous solution by synthesized kaolin supported nanoscale zero-valent iron," *Desalination Water Treat.*, vol. 57, no. 11, pp. 5065–5078, 2016, doi: 10.1080/19443994.2014.1002430.
- [28] I. C. Gerber and P. Serp, "A Theory/Experience Description of Support Effects in Carbon-Supported Catalysts," *Chemical Reviews*, vol. 120, no. 2, pp. 1250-1349, Jan. 2020, doi: 10.1021/acs.chemrev.9b00209.
- [29] Á. Fernández-Galiana, O. Bibikova, S. Vilms Pedersen, y M. M. Stevens, "Fundamentals and Applications of Raman-Based Techniques for the Design and Development of Active Biomedical Materials," *Adv. Mater.*, 2023, p. 2210807, doi: 10.1002/adma.202210807.
- [30] R. S. Das y Y. K. Agrawal, "Raman spectroscopy: Recent advancements, techniques and applications," *Vibrational Spectroscopy*, vol. 57, no. 2, pp. 163–176, 2011, doi: 10.1016/j.vibspec.2011.08.003.
- [31] A. Liu, J. Liu, J. Han, y W.-X. Zhang, "Evolution of nanoscale zero-valent iron (nZVI) in water: Microscopic and spectroscopic evidence on the formation of nano- and micro-structured iron oxides," *Journal of Hazardous Materials*, vol. 322, Part A, pp. 129–135, 2017, doi: 10.1016/j.jhazmat.2015.12.070.
- [32] F. Jiménez, F. Mondragón, y D. López, "Raman characterization of coal carbonizates obtained in a pressurized fixed bed reactor," *Eng. Competitiveness*, vol. 14, no. 2, pp. 111–118, 2012. [Online]. Available: [http://www.scielo.org.co/scielo.php?script=sci\\_arttext&pid=S0123-30332012000200010&lng=en&nrm=iso&tlng=es](http://www.scielo.org.co/scielo.php?script=sci_arttext&pid=S0123-30332012000200010&lng=en&nrm=iso&tlng=es)
- [33] H. Mansour, H. Letifi. R. Bargougui, S. Almeida, B. Negulescu, C. Autret, A. Gadri y S. Ammar, "Structural, optical, magnetic and electrical properties of hematite ( $\alpha$ -Fe<sub>2</sub>O<sub>3</sub>) nanoparticles synthesized by two methods: polyol and precipitation." *Applied Physics A Appl. Phys. A*, vol. 123, 787, 2017. [Online]. Available: <https://link.springer.com/article/10.1007/s00339-017-1408-1>
- [34] Y. Liu, B. Cheng, K. Wang, G. Ling, J. Cai, C. Song, G. Han, "Study of Raman spectra for  $\gamma$ -Al<sub>2</sub>O<sub>3</sub> models by using first-principles methods," *Solid State Commun.*, vol. 178, pp. 16–22, Jan. 2014, doi: 10.1016/j.ssc.2013.09.030.
- [35] I. E. Wachs, "Raman and IR studies of surface metal oxide species on oxide supports: Supported metal oxide catalysts," *Catalysis Today*, vol. 27, pp. 437–455, 1996, doi: 10.1016/0920-5861(95)00203-0
- [36] S. Hua, J.-L. Gong, G.-M. Zeng, F.-B. Yao, M. Guo, y X.-M. Ou, "Remediation of organochlorine pesticides contaminated lake sediment using activated carbon and carbon nanotubes," *Chemosphere*, vol. 177, pp. 65–76, 2017, doi: 10.1016/j.chemosphere.2017.02.133.
- [37] S. Zhang, Y. He, L. Wu, J. Wan, M. Ye, T. Long, Z. Yan, X. Jiang, Y. Lin, y X. Lu, "Remediation of organochlorine pesticide-contaminated soils by surfactant-enhanced washing combined with activated carbon selective adsorption," *Pedosphere*, vol. 29, no. 3, pp. 400–408, 2019, doi: 10.1016/S1002-0160(17)60328-X.
- [38] S. Zhang, Y. He, L. Wu, J. Wan, M. Ye, T. Long, Z. Yan, X. Jiang, G. Xu, P. Yang, S. Yang, H. Wang, y B. Fang, "Non-natural catalysts for catalytic tar conversion in biomass gasification technology," *International Journal of Hydrogen Energy*, vol. 47, no. 12, pp. 7638–7665, 2022, doi: 10.1016/j.ijhydene.2021.12.094.
- [39] E. S. Lokteva, M. D. Pesotskiy, E. V. Golubina, K. I. Maslakov, V. V. Shishova, Yu. Kaplin, S. V. Maksimov, "Effect of Iron Content in Alumina-Supported Palladium Catalysts and Their Reduction Conditions on Diclofenac Hydrodechlorination in an Aqueous Medium," *Kinetics and Catalysis*, vol. 65, pp. 133–154, 2024, doi: 10.1134/S0023158423601183.